Overstretching of a 30 bp DNA duplex studied with steered molecular dynamics simulation: Effects of structural defects on structure and force-extension relation*

H. Li and T. Gisler[a]

Universität Konstanz, Fachbereich Physik, 78457 Konstanz, Germany

Received 15 January 2009 and Received in final form 7 July 2009

Abstract. Single-molecule experiments on polymeric DNA show that the molecule can be overstretched at nearly constant force by about 70% beyond its relaxed contour length. In this publication we use steered molecular dynamics (MD) simulation to study the effect of structural defects on force-extension curves and structures at high elongation in a 30 base pair duplex pulled by its torsionally unconstrained 5′-5′ ends. The defect-free duplex shows a plateau in the force-extension curve at 120 pN in which large segments with inclined and paired bases ("S-DNA") near both ends of the duplex coexist with a central B-type segment separated from the former by small denaturation bubbles. In the presence of a base mismatch or a nick, force-extension curves are very similar to the ones of the defect-free duplex. For the duplex with a base mismatch, S-type segments with highly inclined base pairs are not observed; rather, the overstretched duplex consists of B-type segments separated by denaturation bubbles. The nicked duplex evolves, via a two-step transition, into a two-domain structure characterized by a large S-type segment coexisting with several short S-type segments which are separated by short denaturation bubbles. Our results suggest that in the presence of nicks the force-extension curve of highly elongated duplex DNA might reflect locally highly inhomogeneous stretching.

1 Introduction

Single-molecule stretching experiments on polymeric duplex DNA with several 10^4 base pairs (bp) show that the molecule can be overstretched by up to 70% beyond its natural contour length at nearly constant force of about 50–110 pN [1,2]. The overstretching force depends on ionic strength [3,4], the relative contents of dG-dC and dA-dT pairs [5], on the presence of torsional constraints [6,7], but is independent of pulling velocity [5], indicating that at the low loading rates typically used in experiments on λ-DNA, overstretching occurs at equilibrium. The structural origin of the force plateau has been a matter of some debate: Athermal molecular modelling of duplexes under external force shows, depending on whether the duplex is pulled by the 5′-5′, 3′-3′ or the 5′-3′ ends, underwound ladder or double-helical conformations with paired nucleobases which were termed "S-DNA" [8]. The high tilt of the base pairs in these structures is in line with an early report of force-induced birefringence change in macroscopic DNA fibers [9], fluorescence depolarization of intercalated dyes [10] and molecular dynamics simulations on DNA oligomers [11–13]. However, the force-extension curves of the 12 bp oligomers reported in [11,12] disagree with AFM data which show that short duplexes with less than 30 bp unbind before reaching a force plateau [14,15]. Recent AFM measurements on 30 bp duplexes show that a force plateau at 65 pN, which depends weakly on loading rate, can be observed with sufficiently high force resolution [16].

An alternative explanation for the plateau in the force-extension curve in terms of a force-induced denaturation was put forward by Rouzina *et al.* on the basis of the dependence of the plateau force on temperature and salt concentration [17,18]. In line with this denaturation scenario, molecular dynamics simulations on 12 bp oligomers have indicated the entropic instability of S-DNA resulting from the strongly increased flexibility of the molecule at high extension [19]: while S-type structures with highly tilted and paired nucleobases are observed during simulated overstretching of 12 bp oligomers at high loading rate, pinned simulations starting from highly extended structures show unbinding within about

e-mail: Thomas.Gisler@uni-konstanz.de

4 ns. Direct experimental support for the equilibrium denaturation scenario has very recently been provided by measurements of force-extension curves on λ-DNA in the presence of glyoxal, a reagent which prevents reannealing of broken base pairs by the formation of stable adducts to guanine [20]. Force-extension curves measured after reaction with glyoxal in the extended state show that a large fraction of force-denatured segments are indeed permanently single-stranded.

When the DNA is nicked, the overstretching transition in λ-DNA occurs at a force of about 65 pN irrespective of whether the ends of the duplex are torsionally constrained or not [7], indicating that a nick is sufficient to relax all torsional constraints. Nevertheless, it remains unclear whether the similarity between the force-extension curves of nicked DNA for different end attachment conditions reflects a structural similarity. In particular for high loading rates where the pulling pathway is expected to influence the resulting structure [21,22], the presence of defects should influence the structure of overstretched DNA.

On the other hand, experiments on λ-DNA with torsionally unconstrained ends are usually performed without explicit control over defects along the sugar-phosphate backbone, and it is thus not clear whether the presence or absence of nicks in DNA with torsionally unconstrained ends leads to different internal structures in highly extended duplexes.

In this publication we study the effect of defects on the force-extension curve and structure of a 30 bp DNA duplex pulled by its 5′-5′ ends, using steered MD simulation. For the defect-free duplex, the force-extension curve shows a clear plateau at 120 pN for the lowest stretching velocity $v = 0.1$ nm/ns. In the force plateau, segments with highly inclined and paired nucleobases at both ends of the molecule coexist with a central segment with B-type conformation. B- and S-segments are separated by short denatured segments.

In the presence of a base mismatch or a nick at the center of the molecule the force-extension curves are very similar to the ones of the defect-free duplex. In the mismatched duplex, however, S-type segments are absent and B-type segments coexist with small denaturation bubbles up to very high extensions. In the presence of a nick, the duplex shows a distinct two-stage transition: at moderate elongations, a large segment in B conformation coexists with short B-type segments separated by short denaturation bubbles; at high elongations, the B-type segments show a second transition to an S-type conformation with paired, highly tilted bases.

2 Simulation methods and data analysis

The software package 3xDNA [23] was used to create the initial structure of the 30 bp DNA duplex. The sequence of the duplex (strand 1: 5′-TATCCCACTACCGAGATATCCGCACCAACG-3′) is identical to the one studied in the single-molecule experiments of Morfill *et al.* [16]. We label the bases with the index m running from $m = 1$ at the 5′-T to the 3′-G of strand 1 and back from the 5′-C to the 3′-A end of strand 2. A nick is produced by removing a P atom and the two O atoms not involved in the backbone in the center of strand 1 between G15 and A14 which are subsequently relabelled as terminal bases. A base mismatch is produced by replacing G15 with A15 in strand 1, disrupting the pairing to C46 on strand 2. Simulations were carried out using the MD software package GROMACS 3.3 [24], imported AMBER2003 force fields [25] and the Tip3P water model [26]. The initial DNA duplex was solvated in a cubic box of $4\times4\times20\,\mathrm{nm}^3$. An appropriate number of K^+ ions was added to provide electroneutrality. The O5′ atoms of the two strands were connected to harmonic springs with stiffness $k = 100\,\mathrm{kJ/mol\,nm}^2$. Force was applied by moving the clamped ends of the two springs ($i = 1, 2$) in opposite directions with constant velocity v to positions

$$Z_i(t) = z_i(0) \pm vt, \tag{1}$$

where $z_i(0)$ is the initial position of the end of the molecule. The forces $f_i(t)$ at the two ends were measured at every time step by the relation

$$f_i(t) = k\,(z_i(t) - Z_i(t))\,. \tag{2}$$

Displacing both ends simultaneously has the advantage of reducing friction, as the center of the molecule remains stationary. In the following we report the mean force $f(t) = (f_1(t)+f_2(t))/2$ smoothed by a sliding average over 2000 data points (corresponding to 2 ps).

The distance between complementary nucleobases, $d(m,t)$, was calculated by the mean distance between the atoms involved in the hydrogen bond (*e.g.*, N1, N2 and O6 for guanine). A hydrogen bond was considered broken if the distance between complementary bases was larger than 0.35 nm, a typical length of hydrogen bonds.

The tilt of each nucleobase was quantified by the angle $\theta(m,t)$ between the vector normal to the plane of nucleobase m and the z-axis.

The onset and width of the force plateau as well as the plateau force (for the low pulling velocities only) was determined by fitting a piecewise linear function to the raw $f(t)$ curves (see inset in fig. 1).

3 Results

3.1 Overstretching of a defect-free 30 bp duplex

Figure 1 shows the mean forces $f(l)$ as a function of the end-to-end distance $l = |z_1(t) - z_2(t)|$ obtained with stretching velocities $0.1\,\mathrm{nm/ns} \le v \le 10\,\mathrm{nm/ns}$ for the defect-free 30 bp duplex. With the highest velocity $v = 10$ nm/ns the molecule is stretched to an end-to-end distance $l = 20$ nm within 1 ns. The force increases almost linearly with the extension with a slope of about 60 pN/nm. When the stretching velocity is decreased to 2 nm/ns, we observe a region of end-to-end distance $12.4\,\mathrm{nm} \le l \le 16\,\mathrm{nm}$ where the force increases more weakly with distance (slope of about 14 pN/nm). While in the simulations with

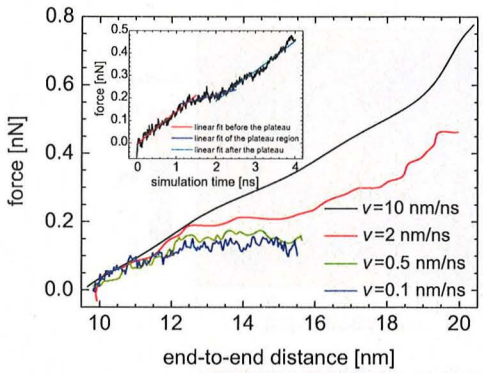

Fig. 1. (Colour on-line) Mean force $f(l)$ at the ends of the defect-free 30 bp DNA duplex as a function of the end-to-end distance $l = |z_1(t) - z_2(t)|$ for different stretching velocities. Inset: raw force $f(t)$ as a function of simulation time t for stretching velocity $v = 2\,\mathrm{nm/ns}$. Linear least-squares fits of a piecewise linear function (colored straight lines) were used to determine the onset and the width of the plateau as well as the plateau force.

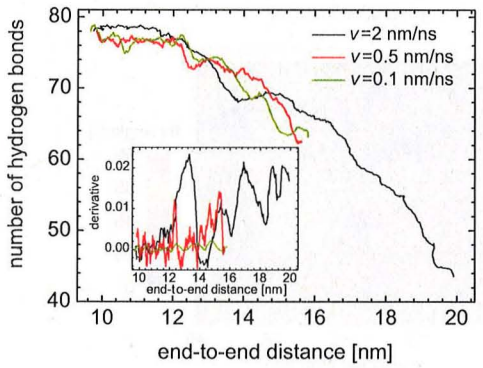

Fig. 2. (Colour on-line) Number of hydrogen bonds $n_{\mathrm{hb}}(l)$ of the defect-free 30 bp duplex as a function of the end-to-end distance l for different stretching velocities. Inset: derivative $\mathrm{d}n_{\mathrm{hb}}/\mathrm{d}l$. The peaks indicate cooperative formation of denaturation bubbles involving several base pairs.

the stretching velocities $v = 0.5\,\mathrm{nm/ns}$ and $v = 0.1\,\mathrm{nm/ns}$ the maximal end-to-end distance was reduced to 16 nm in order to save computation time, force plateaus are clearly visible for $12.4\,\mathrm{nm} \leq l \leq 16\,\mathrm{nm}$. The slopes in the plateau region are very small ($-0.6\,\mathrm{pN/nm}$ for $v = 0.5\,\mathrm{nm/ns}$ and $0.3\,\mathrm{pN/nm}$ for $v = 0.1\,\mathrm{nm/ns}$). Plateau forces are observed to slightly decrease with decreasing stretching velocity.

Figure 2 shows the evolution of the number of hydrogen bonds, $n_{\mathrm{hb}}(l)$, of the defect-free 30 bp duplex with increasing extension. For small $l < 12.6\,\mathrm{nm}$ corresponding to the initial, strong increase in the force-extension curve, n_{hb} remains almost constant for all stretching velocities studied. At larger extensions which correspond to the plateau in $f(l)$ (see fig. 1), $n_{\mathrm{hb}}(l)$ is observed to decrease in steps of about 5 to 10 base pairs. These steps become smaller with smaller stretching velocity (see inset in fig. 2). At the end of the force plateau at $l \approx 16\,\mathrm{nm}$ the number of hydrogen bonds is reduced to about 80%. As the hydrogen bonds in the duplex are almost entirely localized between the complementary nucleobases, the reduction of $n_{\mathrm{hb}}(l)$ indicates the loss of base pairing with increasing force.

Detailed information on the location of the denatured base pairs and their evolution during stretching is revealed by a plot of the distance between the complementary nucleobases, $d(m,t)$, as a function of the base index m and time t (see fig. 3). For $v = 2\,\mathrm{nm/ns}$ a short denatured segment appears at the end of the duplex near $m = 1, 2$ (containing the T-A base pairs) after about 1200 ps which corresponds to the onset of the force plateau. At about 1500 ps, still in the force plateau, two additional short denatured segments near $5 \leq m \leq 7$ and near $24 \leq m \leq 26$ appear. At later times and forces larger than the plateau force, the number of denatured segments increases. Up to about 3800 ps where neighboring denatured segments merge, we observe the nucleation of denatured segments rather than their growth. For the smallest velocity $v = 0.1\,\mathrm{nm/ns}$ the first denatured segments appearing in the force plateau are located at the positions 6 to 9 and 23 to 25 which are similar to the ones observed for larger v.

The tilt angle $\theta(m,t)$ shows high values at both ends of the duplex in the force plateau (see fig. 3). For the lowest stretching velocity, the regions with high tilt angles $\theta(m,t) \geq 50°$ at $m \in [1,8]$ and $m \in [22,30]$ remain localized until the very end of the simulation. Except for the denatured segments, the tilt angle $\theta(m,t)$ is highly symmetric about $m = 30$, in particular in the force plateau (shaded areas in fig. 3), reflecting strong orientation correlation between the complementary nucleobases in a base pair even at high global deformation. For increasing extension, the region of medium tilt angle $20° < \theta < 50°$ grows from the ends of the molecule towards its center; at about 2600 ps, above the force plateau, the last segment with low $\theta \approx 20°$ in the center of the molecule vanishes for $v = 2\,\mathrm{nm/ns}$ (see fig. 3(b)). Comparison with the base distance plot shows that the denatured segments are located at the border between segments with high and with low tilt angle in the force plateau.

Direct inspection of the stretched structure in the force plateau at $l = 14\,\mathrm{nm}$ shows that the high tilt angles in the terminal parts of the duplex are associated with an unwound ladder-like structure with some interstrand stacking interactions (see fig. 4). Near the center, the duplex retains helical twist and the base pairs have low tilt angles. The stacking distance of about 3.4 Å is close to the canonical value for B-DNA. Short denatured segments with about 3 residues separate the regions with high and with low tilt angle.

3.2 Effect of a mismatched base or a nick

Figure 5 shows the force-distance curves for the DNA with a mismatched base and with a nick, respectively. For high stretching velocity $v = 10\,\mathrm{nm/ns}$ no plateau in $f(l)$ is observed. For smaller velocities (2 nm/ns to 0.1 nm/ns),

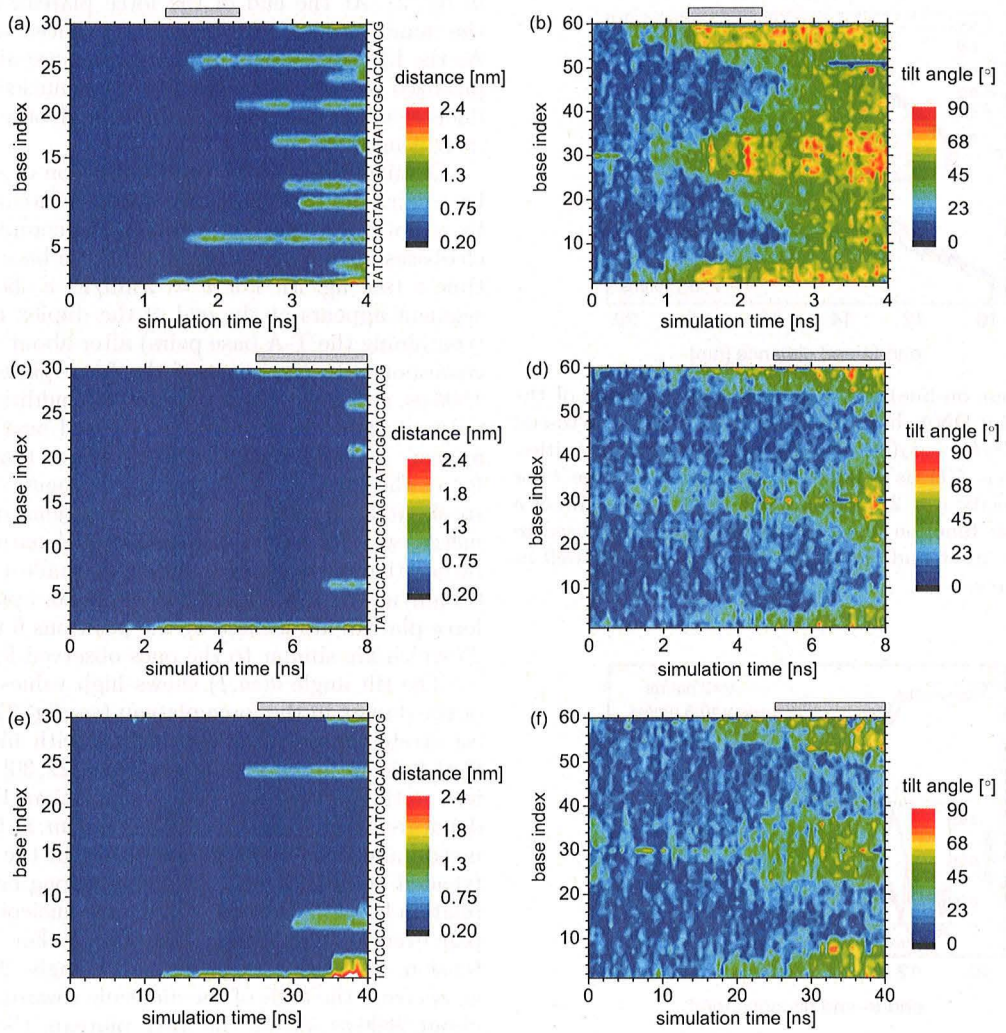

Fig. 3. (Colour on-line) Distance $d(m,t)$ between complementary bases as a function of base index m and time t (a, c, e), and tilt angle $\theta(m,t)$ (b, d, f) of the defect-free 30 bp DNA duplex during stretching with velocities $v = 2\,\mathrm{nm/ns}$ (a, b), $v = 0.5\,\mathrm{nm/ns}$ (c, d) and $v = 0.1\,\mathrm{nm/ns}$ (e, f). The force plateau regions are indicated by the shaded bars.

a force plateau appears for $12.5\,\mathrm{nm} \leq l \leq 16\,\mathrm{nm}$, similar to the situation in the defect-free 30 bp oligomer. Again, the $f(l)$ curves are strongly inclined for high pulling velocities and show a discernible plateau for end-to-end distances of about 12 nm at the smallest pulling velocity.

Figure 6 shows the evolution of the distance $d(m,t)$ between complementary bases and the tilt angle $\theta(m,t)$ for the duplex with the base mismatch. The light blue band around G15 indicates the base pairs which are broken even at low force due to the mismatch. Similar to the situation in the defect-free duplex, persistent denaturation bubbles near the base mismatch and near the end at $m = 30$ appear within the force plateau which are accompanied by large tilt angles. In contrast to the defect-free duplex, we observe no S-type segments with high tilt angles and paired bases in the presence of a base mismatch.

Figure 7 shows that in the duplex with the nick denatured segments appear only in the lower half of the duplex at low pulling velocity (base index $m \in [1, 15]$). Except for the terminal base pairs, the bases in the second, upper half ($m \in [16, 30]$) remain paired during 40 ns simulation. Figure 7(e, f) shows that early in the plateau the upper part of the duplex is a contiguous segment in B conformation, while the lower part ($m < 15$) consists of short B-type segments coexisting with short denaturation bubbles. At high elongations (after about 36 ns) the paired bases show a second transition to an S-type conformation characterized by paired bases with very high tilt, while the denaturation bubbles keep their positions.

This separation into two domains about the nick is illustrated by fig. 8(c, d). The denaturation of the base pairs around the nick allows the lower part of the duplex to untwist under force, while the upper one retains a twisted structure which is very similar to B-DNA. The bases in the lower domain are highly inclined, mainly unpaired and show some inter-strand stacking.

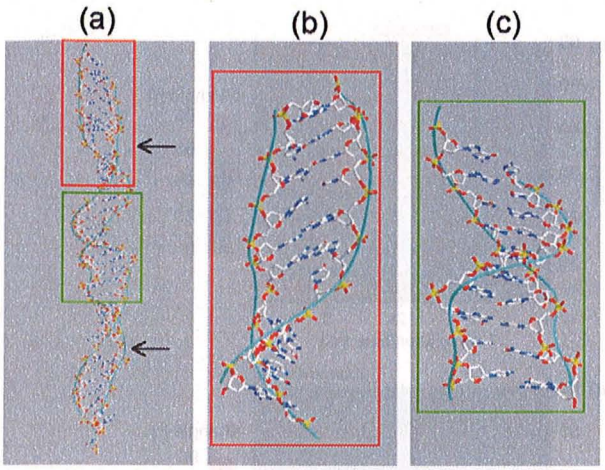

Fig. 4. (Colour on-line) (a) Structure of the defect-free 30 bp duplex stretched to an end-to-end distance $l = 14$ nm with stretching velocity of 0.1 nm/ns. Arrows indicate the denatured segments. Close-ups of the regions delineated by the boxes are shown in (b) and (c). (b) Terminal, unwound part of the stretched 30 bp duplex (base index $m \in [22, 30]$ and $m \in [31, 38]$) with highly inclined bases. (c) Central part of the stretched 30 bp duplex (base index $m \in [11, 20]$ and $m \in [41, 50]$) showing a structure similar to B-DNA. Blue lines: sugar-phosphate backbones of the duplex.

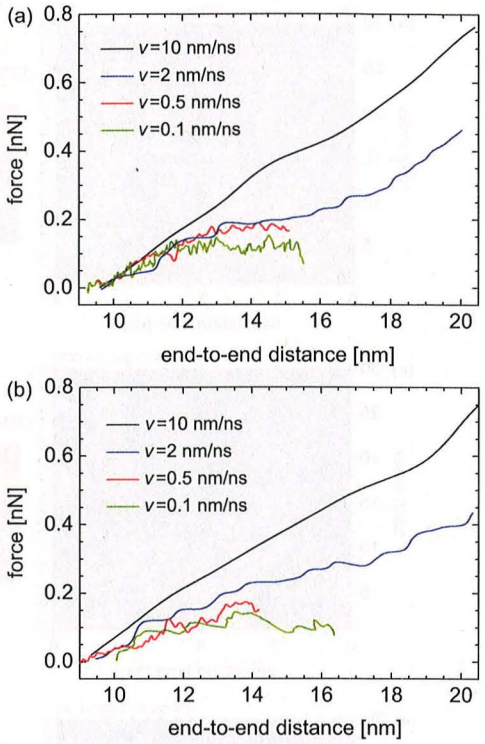

Fig. 5. (Colour on-line) Force-distance curves for a 30 bp DNA with (a) a mismatched base and (b) with a nick.

4 Discussion

Our results show that for the defect-free duplex the base pairing and tilt angles show very similar patterns for the large range of pulling velocities studied here; while the exact position of the denaturation bubbles differs slightly for the different velocities, their occurrence at similar positions near the ends of the duplex indicate that the steered MD simulation does sample typical structures. For the duplexes with the base mismatch and with the nick the base pairing depends more strongly on the pulling velocity. Interestingly, the position of the denaturation bubbles correlate only weakly with the expected "soft spots" at A or T sites. A possible reason for this unexpected behavior could be artefacts introduced by the AMBER2003 force field used here which are known to lead to artificial, irreversible α/γ transitions for simulation times larger than about 10 ns [27]. A comparison of base distance and base tilt plots $d(m,t)$ and $\theta(m,t)$ obtained from steered MD simulations of a 14 bp duplex with AMBER and AMBER99b (equivalent to AMBER2003) and bsc0 [27] force fields over 20 ns and 2 nm/ns pulling velocity showed good agreement (see fig. S1 in supplementary material) and good correlation of the denaturation sites with AT pairs. Stretching simulations for the 30 bp duplex without a defect, with a nick and with a base mismatch using AMBER and the bsc0 force field with pulling at 2 nm/ns for 2 ns force yield structural features which are similar to the ones obtained with the AMBER2003 force field (see fig. S2 in supplementary material). The largest discrepancies between the results of AMBER99b and bsc0 force fields are observed with the nicked duplex. The weak correlation of the denaturation sites with A or T bases which is also obtained with the bsc0 force field might be an intrinsic problem of the latter when simulating larger DNA duplexes.

Our results show that the onset of the force plateau coincides with the formation of denatured segments for the defect-free 30 bp duplex as well as for the duplex with the base mismatch. For the defect-free duplex, the simulations show evidence for a coexistence between segments with high base tilt and intact base pairing (S-DNA) at the ends of the duplex and a central segment with B-type structure which is separated from the former by short denatured segments.

The stretching velocities used in the present simulations which are by a factor of about 10^5 larger than the ones used in the experiments [16] are reflected by the high value of the plateau force which is by a factor of about 2 larger than the 65 pN observed in the AFM experiments on the oligomers with identical sequence. The plateau force of 110 pN observed in defect-free λ-DNA with 5′ and 3′ ends of both strands attached to the substrates [7] have suggested that the low plateau force of 65 pN might be associated with the relaxation of torsion in the presence of nicks. In our simulations, we observe a monotonous, velocity-independent reduction of the average twist angle from 33° in the relaxed duplex to 24° at an end-to-end distance $l = 15$ nm, indicating that the torsion is relaxed during stretching (see fig. S3 in supplementary material). This suggests that the high plateau forces of about 120 pN

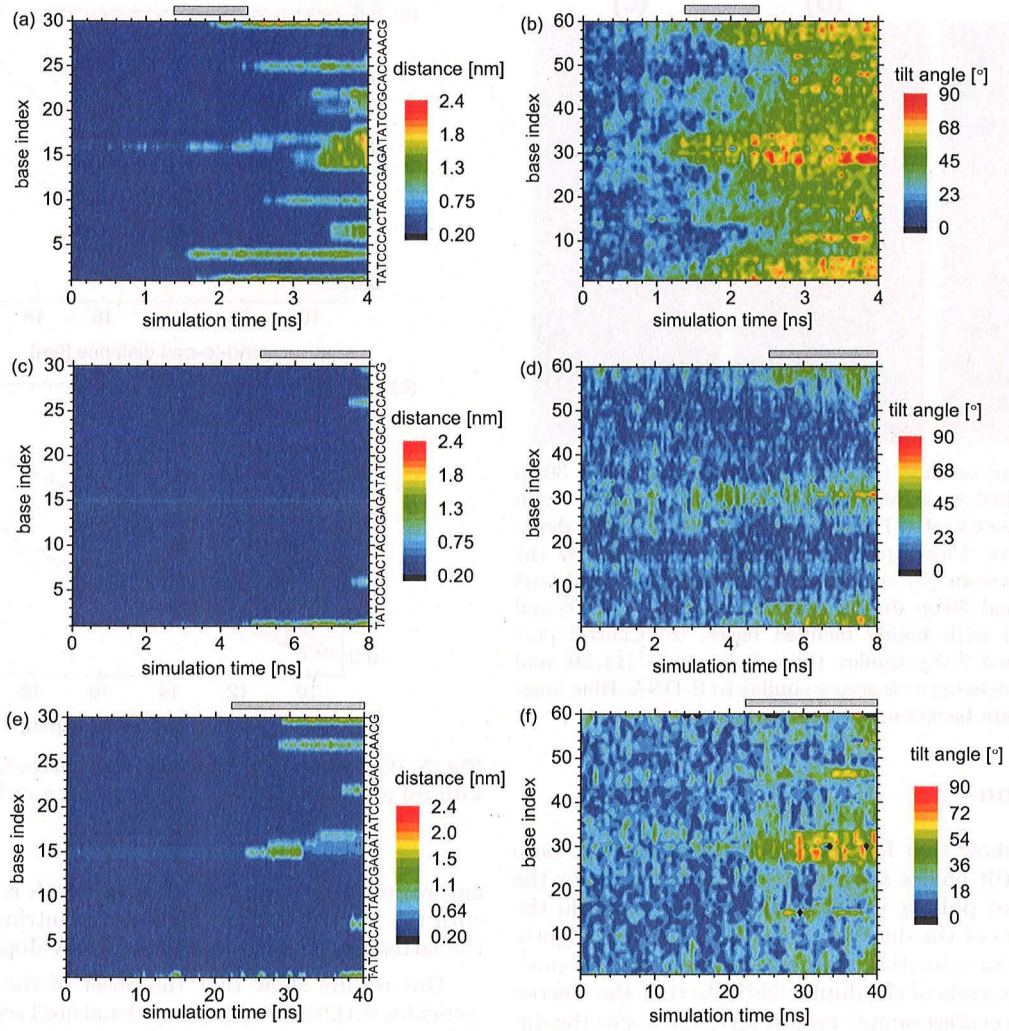

Fig. 6. (Colour on-line) Distance $d(m,t)$ between complementary bases as a function of base index m and time t (a, c, e), and tilt angle $\theta(m,t)$ (b, d, f) of the 30 bp DNA duplex with a mismatched base during stretching with velocities $v = 2\,\mathrm{nm/ns}$ (a, b), $v = 0.5\,\mathrm{nm/ns}$ (c, d) and $v = 0.1\,\mathrm{nm/ns}$ (e, f). The force plateau regions are indicated by the shaded bars.

observed in our simulations are unlikely due to unrelaxed twist.

The onset of the plateau observed for the lowest stretching velocities is at about 12.4 nm, as measured by the extrapolation of the linear $f(l)$ relations in the plateau and at low forces. This value is by about 27% larger than the relaxed contour length $l_0 = 9.8\,\mathrm{nm}$ which is determined from equilibrium simulations. Experiments on polymeric DNA show that the onset of the plateau is separated from the low-force regime by a high-force Hookean range which is, if normalized to the relaxed contour length, considerably narrower than observed here. Unfortunately, the onset of the force plateau is difficult to estimate from the available AFM data on the 30 bp oligomers due to the presence of the very flexible PEG spacer [16], making a comparison of force-extension curves at low forces difficult. The width of the plateau we observe for the lowest stretching velocities is at least 3.6 nm, corresponding to an overstretching of about 63%. As our simulations were restricted in length, the actual width of the plateau might be larger.

Our results show that, although the force-extension curves for defect-free 30 bp oligomers are qualitatively and quantitatively similar (albeit not identical) to the ones of duplexes with a nick or a base mismatch, the force-induced structural changes in the presence of a defect differ strongly even though the ends are torsionally unconstrained. In the presence of the nick, stretching induces a two-domain structure at the highest elongations, one part being a contiguous segment in S conformation, the other consisting of short S-type segments separated by short denaturation bubbles. This two-domain structure originates in the asymmetry between the two strands: due to the nick in strand 2 (base index $m \in [31, 60]$), its upper part is not under tension and allows to stabilize, by hydrogen bonds to the complementary bases on strand 1, the

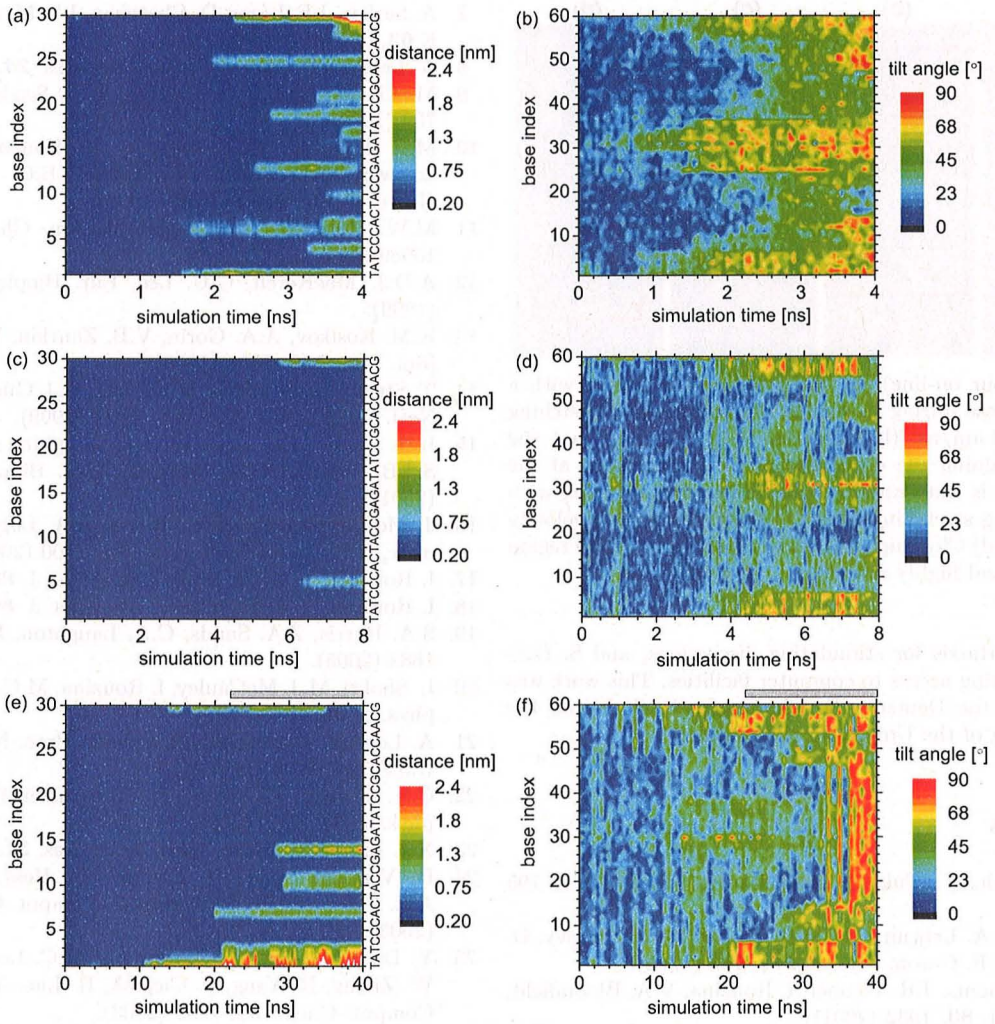

Fig. 7. (Colour on-line) Distance $d(m,t)$ between complementary bases as a function of base index m and time t (a, c, e), and tilt angle $\theta(m,t)$ (b, d, f) of the 30 bp DNA duplex with a nick at residue 15 during stretching with velocities $v = 2\,\mathrm{nm/ns}$ (a, b), $v = 0.5\,\mathrm{nm/ns}$ (c, d) and $v = 0.1\,\mathrm{nm/ns}$ (e, f). The force plateau regions are indicated by the shaded bars.

unwound S-type conformation in the upper part of the duplex.

The velocity dependence of the plateau force indicates that the structures induced by the stretching are not equilibrated. On the other hand, the stress propagation is almost instantaneous: assuming the speed of sound in DNA to be about 3000 m/s [28], the stress propagates along the length of the duplex in about 7–10 ps. The persistent denaturation bubbles observed in our simulations are thus likely to originate from nucleation centers whose growth is much slower, being determined by dissipation rather than by stress propagation. We thus speculate that S-type segments, coexisting with denaturation bubbles, might —even if thermodynamically unstable— be kinetically trapped in much longer DNA, such as λ, even at the far lower pulling velocities realized in optical tweezer experiments.

5 Conclusions

In conclusion, we have shown that the presence of a nick or a mismatched nucleobase in a 30 bp duplex DNA with torsionally unconstrained ends results in force-extension curves which are quantitatively very similar to the ones of a defect-free duplex. In contrast, the structures observed differ strongly from each other at high extensions. While the results shown here are on a duplex which is extended via its 5′-5′ ends, further simulations on a duplex extended via the 3′-3′ ends might elucidate the recently found differences between these pulling modalities at high loading rates [22]. Experiments on polymeric DNA with deliberately positioned defects might, on the other hand, provide additional information on the conformation within the segments with remaining base pairing.

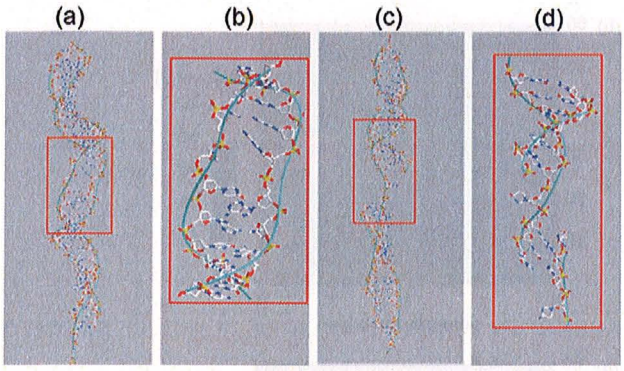

Fig. 8. (Colour on-line) (a) Structure of the duplex with a mismatched base during stretching after 25 ns with stretching velocity of 0.1 nm/ns. (b) Close-up of (a) showing that the segment containing the denaturation bubble centered at the mismatch site is untwisted. (c) Structure of the duplex with the nick during stretching after 25 ns with stretching velocity of 0.1 nm/ns. (d) Close-up of (c) showing that the nicked region is denatured and highly stretched.

We thank S. Harris for stimulating discussions, and S. Gerlach for providing access to computer facilities. This work was supported by the Deutsche Forschungsgemeinschaft and the Zukunftskolleg of the University of Konstanz.

References

1. S.B. Smith, Y. Cui, C. Bustamante, Science **271**, 795 (1996).
2. P. Cluzel, A. Lebrun, C. Heller, R. Lavery, J.L. Viovy, D. Chatenay, F. Caron, Science **271**, 792 (1996).
3. M.C. Williams, J.R. Wenner, I. Rouzina, V.A. Bloomfield, Biophys. J. **80**, 1932 (2001).
4. M.C. Williams, J.R. Wenner, I. Rouzina, V.A. Bloomfield, Biophys. J. **80**, 874 (2001).
5. M. Rief, H. Clausen-Schaumann, H.E. Gaub, Nature Struct. Biol. **6**, 346 (1999).
6. H. Clausen-Schaumann, M. Rief, C. Tolksdorf, H.E. Gaub, Biophys. J. **78**, 1997 (2000).
7. A. Sarkar, J.F. Léger, D. Chatenay, J.F. Marko, Phys. Rev. E **63**, 051903 (2001).
8. A. Lebrun, R. Lavery, Nucl. Acids Res. **24**, 2260 (1996).
9. M.H.F. Wilkins, R.G. Gosling, W.E. Seeds, Nature **167**, 759 (1951).
10. M.L. Bennink, O.D. Schärer, R. Kanaar, K. Sakata-Sogawa, J.M. Schins, J.S. Kanger, B.G. de Grooth, J. Greve, Cytometry **36**, 200 (1999).
11. M.W. Konrad, J.I. Bolonick, J. Am. Chem. Soc. **118**, 10989 (1996).
12. A.D.J. MacKerell, G.U. Lee, Eur. Biophys. J. **28**, 415 (1999).
13. K.M. Kosikov, A.A. Gorin, V.B. Zhurkin, W.K. Olson, J. Mol. Biol. **289**, 1301 (1999).
14. T. Strunz, K. Orozslan, R. Schäfer, H.J. Güntherodt, Proc. Natl. Acad. Sci. U.S.A. **96**, 11277 (1999).
15. L.H. Pope, M.C. Davies, C.A. Laughton, C.J. Roberts, S.J.B. Tendler, P.M. Williams, Eur. Biophys. J. **30**, 53 (2001).
16. J. Morfill, F. Kühner, K. Blank, R.A. Lugmaier, J. Sedlmair, H.E. Gaub, Biophys. J. **93**, 2400 (2007).
17. I. Rouzina, V.A. Bloomfield, Biophys. J. **80**, 882 (2001).
18. I. Rouzina, V.A. Bloomfield, Biophys. J. **80**, 894 (2001).
19. S.A. Harris, Z.A. Sands, C.A. Laughton, Biophys. J. **88**, 1684 (2005).
20. L. Shokri, M.J. McCauley, I. Rouzina, M.C. Williams, Biophys. J. **95**, 1248 (2008).
21. A. Lebrun, Z. Shakked, R. Lavery, Proc. Natl. Acad. Sci. U.S.A. **94**, 2993 (1997).
22. C.H. Albrecht, G. Neuert, R.A. Lugmaier, H.E. Gaub, Biophys. J. **94**, 4766 (2008).
23. X.J. Lu, W.K. Olson, Nucl. Acids Res. **31**, 5108 (2003).
24. D. Van der Spoel, E. Lindahl, B. Hess, G. Groenhof, A.E. Mark, H.J.C. Berendsen, J. Comput. Chem. **26**, 1701 (2005).
25. Y. Duan, C. Wu, S. Chowdhury, M.C. Lee, G.M. Xiong, W. Zhang, R. Yang, P. Cieplak, R. Luo, T. Lee *et al.*, J. Comput. Chem. **24**, 1999 (2003).
26. D.J. Price, C.L. Brooks, J. Chem. Phys. **121**, 10096 (2004).
27. A. Pérez, I. Marchán, D. Svozil, J. Sponer, T.E. Cheatham III, C.A. Laughton, M. Orozco, Biophys. J. **92**, 3817 (2007).
28. F. Merzel, F. Fontaine-Vive, M.R. Johnson, G.J. Kearley, Phys. Rev. E **76**, 031917 (2007).